On Prediction of 3d Stress State in Elastic Shell by Higher-order Shell Formulations

Boštjan Brank[1]**, Adnan Ibrahimbegovic**[2] **and Uroš Bohinc**[3]

Abstract: In this work we study the accuracy of modern higher-order shell finite element formulations in computation of 3d stress state in elastic shells. In that sense we compare three higher-order shell models: (i) with seven displacement-like kinematic parameters, and (ii, iii) with six displacement-like kinematic parameters plus one strain-like kinematic parameter introduced by two different versions of enhanced assumed strain (EAS) concept. The finite element approximations of all shell models are based on 4-node quadrilateral elements. Geometrically nonlinear and consistently linearized forms of considered formulations are given. Several numerical examples are presented, where computed stresses are compared with analytical solutions. It was found that through-the-thickness variation of some (non-dominant) stress tensor components, including through-the-thickness normal stress, may be computed very inaccurately. The reliable representation for those stresses can be interpreted only if the "layer-wise" averaging or the through-the-thickness averaging is performed.

Keyword: higher-order shell model, 3d constitutive equations, stress computation

1   Introduction

During the recent years several higher-order shell models, accounting for through-the-thickness stretch, have been presented along with their finite element approximations. The main motivation behind is development of effective shell formulation that can use fully three-dimensional (3d) constitutive model (with no modifications with respect to 3d continuum mechanics). The most effective approach to achieve

[1] University of Ljubljana, Faculty of Civil and Geodetic Engineering, Jamova 2, 1000 Ljubljana, Slovenia

[2] Ecole Normale Supérieure de Cachan, LMT, 61, av. du President Wilson, 94235 Cachan cedex, France

[3] Slovenian National Building and Civil Engineering Institute, Dimičeva 12, 1000 Ljubljana, Slovenia

that goal is a refinement of the standard shell model of Reissner-Mindlin type, which is commonly used for plate and shell analysis [Tonković, Sorić and Skozrit (2008); Wen and Hon (2007)]. Such refinement has been effectively performed on the level of kinematics.

The kinematic refinement has been achieved either by refining the kinematic assumption of the standard shell model of Reissner-Mindlin type, or by modifying the 8-node solid element in order to include the shell-like features in one direction. The first approach is sometimes called *3-d shell* and the second one *solid-shell* [Kulikov and Plotnikova (2008)]. Examples of the first approach, which will be considered in what follows, are given e.g. in Büchter, Ramm and Roehl (1994); Sansour (1995); Bischoff and Ramm (1997); Eberlein and Wriggers (1999); Betsch, Gruttmann and Stein (1996); Başar, Itskov and Eckstein (2000); Brank, Korelc and Ibrahimbegovic (2002); Krätzig and Jun (2003); Brank (2005).

All the above works have been concerned that newly developed higher-order shell formulations behave correctly for thin shells. The correctness has been estimated numerically, through engineering judgement and by mathematical proof, although the latter has been given only for (1,1,2)-plate model [Rossle, Bischoff, Wendland and Ramm (1999)]. Numerical estimations have been related to comparison of computed displacements with analytical and other available solutions. Special attention has been given to evaluation of results of higher-order shell formulations for thin shells. However, no comparison of stresses or stress resultants has been made to reference values.

In this work we study the following question: How good are the 3-d shell formulations in representing the 3d stress state in an elastic shell-like body? In that sense the following higher-order shell models are considered: (i) a 7-parameter shell model with 3 displacements of the mid-surface, 2 rotations of shell director (see e.g. Atluri and Cazzani (1995), Brank and Ibrahimbegovic (2001) Lin (2006) for discussions on finite rotations), and 2 thickness-stretching parameters; (ii) a 7-parameter shell model with the first 6 parameters equal to those of (i), while the 7th parameter is a through-the-thickness strain, introduced with the enhanced assumed strain concept (EAS) and an assumption of additive decomposition of strains [Simo and Rifai (1990)]; (iii) a 7-parameter shell model where the introduction of the 7th parameter is based on additive decomposition of displacement gradient [Simo and Armero (1992)], leading to the multiplicative decomposition of strains.

Geometrically nonlinear formulations are first derived. Their consistent linearized forms are then obtained in order to study geometrically linear problems. The question on stress accuracy has been answered by computation of several illustrative examples and by comparison of obtained results with analytical solutions from linear elasticity.

2 Higher-order shell (3-d shell) formulations

In this section we will briefly present three versions of 3-d shell model. Those versions differ from each other by the approach used to refine standard Reissner-Mindlin shell kinematics in order to get a formulation which can use fully 3-d constitutive equations in the appropriate way.

2.1 Version 1 of 3-d shell formulation

Let us define position of a shell point in the initial configuration with respect to fixed Cartesian frame as

$$\mathbf{X}\left(\xi^1,\xi^2,\xi\right) = \boldsymbol{\varphi}_0\left(\xi^1,\xi^2\right) + \xi\mathbf{g}\left(\xi^1,\xi^2\right) \tag{1}$$

$$\|\mathbf{g}\| = 1, \quad \left(\xi^1,\xi^2\right) \subset \mathscr{A} \subset \mathbb{R}^2,$$
$$\xi = h_0/2\zeta, \quad \zeta \in [-1,\ 1]$$

where ξ^1,ξ^2 are curvilinear coordinates parametrizing the mid-surface, ξ and ζ are through-the-thickness coordinates, $\boldsymbol{\varphi}_0$ is position of the corresponding point on the mid-surface, h_0 is constant initial thickness, $\mathscr{A}$ is domain of the mid-surface parametrization, and $\mathbf{g}$ is normal to the mid-surface (shell director). We assume that position of the same point in deformed configuration is given as

$$\mathbf{x}\left(\xi^1,\xi^2,\xi\right) = \boldsymbol{\varphi}\left(\xi^1,\xi^2\right) + \xi\underbrace{\lambda\left(\xi^1,\xi^2\right)\mathbf{a}\left(\vartheta\left(\xi^1,\xi^2\right)\right)}_{\mathbf{d}(\xi^1,\xi^2)}$$

$$+ (\xi)^2\underbrace{q\left(\xi^1,\xi^2\right)\mathbf{a}\left(\vartheta\left(\xi^1,\xi^2\right)\right)}_{\mathbf{f}(\xi^1,\xi^2)} \tag{2}$$

where $\boldsymbol{\varphi} = \boldsymbol{\varphi}_0 + \mathbf{u}$ is current position of the mid-surface, $\mathbf{u}$ is mid-surface displacement, $\mathbf{a}$, $\|\mathbf{a}\| = 1$, is rotated $\mathbf{g}$ defined by two finite rotation parameters $\boldsymbol{\vartheta} = \left[\vartheta^1, \vartheta^2\right]^T$, $\lambda = h/h_0$, q are two thickness stretching parameters, and h is current thickness. In what follows we replace λ with $\widetilde{\lambda} = \lambda - 1$.

The Green-Lagrange strains with respect to the dual basis $\mathbf{g}^i$ (defined such that $\mathbf{g}^i \cdot \mathbf{g}_j = \delta^i_j$, where $\mathbf{g}_j = \partial\mathbf{X}/\partial\xi^j$, and δ^i_j is Kronecker's delta symbol) are

$$E_{ij}\left(\boldsymbol{\Phi}\left(\xi^1,\xi^2\right),\xi\right) = E_{ij}\left(\underbrace{\mathbf{u},\boldsymbol{\vartheta},\widetilde{\lambda},q}_{\boldsymbol{\Phi}(\xi^1,\xi^2)},\xi\right) = \frac{1}{2}\left(\mathbf{x}_{,i}\cdot\mathbf{x}_{,j} - \mathbf{X}_{,i}\cdot\mathbf{X}_{,j}\right) \tag{3}$$

where the notation $(\circ)_{,i} \equiv \partial(\circ)/\partial\xi^i$ and $\xi \equiv \xi^3$ has been introduced. It can be shown that some strains E_{ij} are quadratic, some cubic and some quartic functions

of ξ. In order to have the same order of through-the-thickness variation for all strain tensor components, we make the following truncation

$$E_{ij} \rightarrow E_{ij}\mid_{\xi=0} + \xi \frac{dE_{ij}}{d\xi}\mid_{\xi=0} + \frac{\xi^2}{2}\frac{d^2 E_{ij}}{d\xi^2}\mid_{\xi=0} \tag{4}$$

One can further introduce at each point $\mathbf{X}\left(\xi^1,\xi^2,\xi\right)$ of the shell a local Cartesian frame with the following basis

$$\widehat{\mathbf{e}}_3 = \mathbf{g}, \widehat{\mathbf{e}}_1 \perp \widehat{\mathbf{e}}_3, \widehat{\mathbf{e}}_2 = \widehat{\mathbf{e}}_3 \times \widehat{\mathbf{e}}_1 \tag{5}$$

and define strains at that point with respect to the basis (5) as

$$\widehat{E}_{ij} = T_{ik}E_{kl}T_{jl} \tag{6}$$

where

$$[T_{ij}] = \begin{bmatrix} \mathbf{X}_{,1}\cdot\widehat{\mathbf{e}}_1 & \mathbf{X}_{,1}\cdot\widehat{\mathbf{e}}_2 & 0 \\ \mathbf{X}_{,2}\cdot\widehat{\mathbf{e}}_1 & \mathbf{X}_{,2}\cdot\widehat{\mathbf{e}}_2 & 0 \\ 0 & 0 & 1 \end{bmatrix}^{-1} \tag{7}$$

The potential energy of the hyperelastic shell can be for the St. Venant-Kirchhoff material model written as

$$\Pi\left(\mathbf{\Phi}\right) = \int_V \underbrace{\left(\frac{\Lambda}{2}\left(Tr\left[\widehat{E}_{ij}\right]\right)^2 + \mu Tr\left[\widehat{E}_{ij}\widehat{E}_{ij}\right]\right)}_{W\left(\widehat{E}_{ij}(\mathbf{\Phi},\xi)\right)}dV - \underbrace{\int_A \pi_{ext}\left(\mathbf{\Phi}\right)dA}_{\Pi_{ext}(\mathbf{\Phi})} \tag{8}$$

where Λ and μ are Lame's parameters. V and A are shell volume and mid-surface area at the initial configuration. The external part of the potential energy is (by assuming only conservative pressure loading p^{top} and p^{bot} at top and bottom surfaces of the shell)

$$\pi_{ext} = -p^{top}\mu^{top}\mathbf{g}\cdot\mathbf{u}^{top} + p^{bot}\mu^{bot}\mathbf{g}\cdot\mathbf{u}^{bot} \tag{9}$$

where

$$\mu^{top,bot} = \sqrt{\frac{\left(\mathbf{X}_{,1}^{top,bot}\times\mathbf{X}_{,2}^{top,bot}\right)\cdot\left(\mathbf{X}_{,1}^{top,bot}\times\mathbf{X}_{,2}^{top,bot}\right)}{\left(\boldsymbol{\varphi}_{0,1}\times\boldsymbol{\varphi}_{0,2}\right)\cdot\left(\boldsymbol{\varphi}_{0,1}\times\boldsymbol{\varphi}_{0,2}\right)}} \tag{10}$$

and $\mathbf{u}^{top}$, $\mathbf{u}^{bot}$ are nonlinear functions of kinematic parameters composed in $\mathbf{\Phi}$

$$\mathbf{u}^{top,bot} = \mathbf{u}^{top,bot}\left(\mathbf{\Phi}\right) \quad = \mathbf{u} \pm \frac{h_0}{2}\left(\mathbf{d}\left(\widetilde{\lambda},\mathbf{a}\left(\boldsymbol{\vartheta}\right)\right) - \mathbf{g}\right) + \frac{h_0^2}{4}\mathbf{f}(q,\mathbf{a}\left(\boldsymbol{\vartheta}\right)) \tag{11}$$

It is assumed above that **g** is oriented from the bottom towards the top surface.

The weak form of equilibrium equations can be obtained by introducing the variations for displacement $\mathbf{u} \to \mathbf{u} + \varepsilon\delta\mathbf{u}$, shell director rotation $\mathbf{a}\left(\boldsymbol{\vartheta}\right) \to \mathbf{a}\left(\boldsymbol{\vartheta} + \varepsilon\delta\boldsymbol{\vartheta}\right)$, and thickness stretching parameters $\widetilde{\lambda} \to \widetilde{\lambda} + \varepsilon\delta\widetilde{\lambda}$, $q \to q + \varepsilon\delta q$ into the potential energy expression (8). We thus attain

$$\frac{d\Pi}{d\varepsilon}\mid_{\varepsilon=0} = G\left(\underbrace{\delta\boldsymbol{\Phi}}_{\left\{\delta\mathbf{u},\delta\boldsymbol{\vartheta},\delta\widetilde{\lambda},\delta q\right\}} ; \boldsymbol{\Phi}\right) = 0 \tag{12}$$

The problem is further solved by means of the finite element approximation.

2.2   *Version 2 of 3-d shell formulation*

Let us now assume position of a shell point in deformed configuration relative to fixed Cartesian frame as

$$\mathbf{x}\left(\xi^1,\xi^2,\xi\right) = \boldsymbol{\varphi}\left(\xi^1,\xi^2\right) + \xi\mathbf{d}\left(\xi^1,\xi^2\right) \tag{13}$$

The Green-Lagrange strains with respect to the basis $\mathbf{g}^i$, which are compatible with assumption (13), are

$$E_{ij}^u\left(\boldsymbol{\Phi}_{EAS}\left(\xi^1,\xi^2\right),\xi\right) = E_{ij}^u\left(\underbrace{\mathbf{u},\boldsymbol{\vartheta},\widetilde{\lambda}}_{\boldsymbol{\Phi}_{EAS}(\xi^1,\xi^2)},\xi\right) = \frac{1}{2}\left(\mathbf{x}_{,i}\cdot\mathbf{x}_{,j} - \mathbf{X}_{,i}\cdot\mathbf{X}_{,j}\right) \tag{14}$$

It can be shown that some components of E_{ij}^u are linear and some quadratic functions of ξ, and that E_{33}^u is only constant with respect to ξ. To have all components of the same order, we make the following truncation

$$E_{ij}^u \to E_{ij}^u\mid_{\xi=0} + \xi\frac{dE_{ij}^u}{d\xi}\mid_{\xi=0} \tag{15}$$

and add the missing linear term of E_{33}^u within the framework of the enhanced assumed strain (EAS) concept [Simo and Rifai (1992)]. The crucial part of the EAS concept is assumption that the Green-Lagrange strains are the sum of displacement-compatible strains E_{ij}^u and some enhancing strains $\widetilde{E}_{ij}$. That leads to enhanced strains

$$E_{ij} = E_{ij}^u + \widetilde{E}_{ij} \tag{16}$$

Here we choose such enhancing strains $\widetilde{E}_{ij}$ that all components of the enhanced (total) strains E_{ij} are linear with respect to ξ, i.e.

$$\widetilde{E}_{ij}\left(\alpha_{ij}\left(\xi^1,\xi^2\right),\xi\right) = \begin{cases} \xi\,\alpha_{33}\left(\xi^1,\xi^2\right) & \text{if } i=3 \text{ and } j=3 \\ 0 & \text{otherwise} \end{cases} \tag{17}$$

where α_{ij} are enhancing strain parameters. We collect non-zero parameters in $\boldsymbol{\alpha}$, i.e. $\boldsymbol{\alpha} = \{\alpha_{33}\}$. By using (6), the strains E_{ij} can be transformed to strains $\widehat{E}_{ij} = \widehat{E}^u_{ij} + \widehat{\widetilde{E}}_{ij}$ that are defined with respect to the local Cartesian frame with the basis (5).

Assumption of additive decomposition of total strains (16) is introduced in the Hu-Washizu functional $\Pi_{H-W}\left(\boldsymbol{\Phi}_{EAS},\widetilde{E}_{ij},S^{ij}\right)$, where S^{ij} are the 2nd Piola-Kirchhoff stresses defined with respect to the basis $\mathbf{g}_i$. The following functional is obtained

$$\Pi_{EAS1}\left(\boldsymbol{\Phi}_{EAS},\boldsymbol{\alpha}\right) = \int_V W\left(\widehat{E}^u_{ij}\left(\boldsymbol{\Phi}_{EAS}\left(\xi^1,\xi^2\right),\xi\right) + \widehat{\widetilde{E}}_{ij}\left(\boldsymbol{\alpha}\left(\xi^1,\xi^2\right),\xi\right)\right)dV$$
$$- \Pi_{ext}\left(\boldsymbol{\Phi}_{EAS}\left(\xi^1,\xi^2\right)\right) \tag{18}$$

if the orthogonality between stresses and enhancing strains is assumed to be valid

$$\int_V \widehat{S}^{ij}\widehat{\widetilde{E}}_{ij}dV = \int_V S^{ij}\widetilde{E}_{ij}dV = 0 \stackrel{(17)}{\Rightarrow} \tag{19}$$
$$\int_V S^{33}\widetilde{E}_{33}\,dV = \int_V S^{33}\xi\,\alpha_{33}\,dV = 0$$

Note that $\Pi_{ext}\left(\boldsymbol{\Phi}_{EAS}\right)$ is equal to $\Pi_{ext}\left(\boldsymbol{\Phi}\right)$ defined in (8) to (11), except that the last term in (11) drops out. Since $dV = (1 - 2\xi H + (\xi)^2 K)d\xi dA$, where $H = H\left(\xi^1,\xi^2\right)$ and $K = \left(\xi^1,\xi^2\right)$ are mean and Gaussian mid-surface curvatures, respectively, one can write (19) as

$$\int_V S^{33}\xi\,\alpha_{33}dV = \int_A \alpha_{33}\int_{-h/2}^{h/2} S^{33}\underbrace{(1 - 2\xi H + (\xi)^2 K)}_{\mu}\xi d\xi dA = 0 \tag{20}$$

Equation (20) holds for shells with $\mu \approx 1$ for constant S^{33} stress with respect to ξ coordinate, i.e. for $S^{33} = S^{33}\left(\xi^1,\xi^2\right)$. It also holds for shells with $H = const.$, $K = const.$ for $S^{33} = S^{33}\left(\xi\right)$, if α_{33} is chosen such that $\int_A \alpha_{33}dA = 0$.

One can introduce variations of displacement $\mathbf{u} \to \mathbf{u} + \varepsilon\delta\mathbf{u}$, shell director rotation $\mathbf{a}\left(\boldsymbol{\vartheta}\right) \to \mathbf{a}\left(\boldsymbol{\vartheta} + \varepsilon\delta\boldsymbol{\vartheta}\right)$, thickness stretching parameter $\widetilde{\lambda} \to \widetilde{\lambda} + \varepsilon\delta\widetilde{\lambda}$, and enhancing

strain parameters $\boldsymbol{\alpha} \to \boldsymbol{\alpha} + \varepsilon \delta \boldsymbol{\alpha}$. Those variations are then introduced in Π_{EAS1} to obtain $G_{EAS1} = \frac{d\Pi_{EAS1}}{d\varepsilon}|_{\varepsilon=0}$. At the stationary point

$$G_{EAS1}\left(\underbrace{\delta\boldsymbol{\Phi}_{EAS}}_{\{\delta\mathbf{u},\delta\boldsymbol{\vartheta},\delta\widetilde{\lambda},\delta q\}}, \delta\boldsymbol{\alpha}; \boldsymbol{\Phi}_{EAS}, \boldsymbol{\alpha}\right) = 0 \tag{21}$$

the equilibrium and kinematic relations are fulfilled in a weak form. The functional (21) is further solved for $\boldsymbol{\Phi}_{EAS}$ and $\boldsymbol{\alpha}$ (for any kinematically admissible variations $\delta\boldsymbol{\Phi}_{EAS}$ and $\delta\boldsymbol{\alpha}$) by the finite element approximation. Since $\boldsymbol{\alpha}$ parameters not need to be continuos over the domain, they are condensed on the element level and we recover the standard finite element computer code structure.

2.3 Version 3 of 3-d shell formulation

Let us now assume position of a shell point in deformed configuration relative to fixed Cartesian frame, as in (13), and replace assumption (16) with assumption that total deformation gradient $\mathbf{F}$ is a sum of displacement dependent part $\mathbf{F}^u$ and enhancing part $\widetilde{\mathbf{F}}$

$$\mathbf{F} = \mathbf{F}^u\left(\boldsymbol{\Phi}_{EAS}, \xi\right) + \widetilde{\mathbf{F}} \tag{22}$$

$\widetilde{\mathbf{F}}$ can be defined through the geometrically nonlinear version of incompatible modes method [Ibrahimbegovic and Wilson (1991); Ibrahimbegovic and Frey (1993)], which is equivalent to geometrically nonlinear version of EAS [Simo and Armero (1992)]. Since $\mathbf{F}^u = \mathbf{x}_{,i} \otimes \mathbf{g}^i$, one can assume that

$$\widetilde{\mathbf{F}} = \widetilde{\mathbf{x}}_{,i} \otimes \mathbf{g}^i \implies \mathbf{F} = (\mathbf{x}_{,i} + \widetilde{\mathbf{x}}_{,i}) \otimes \mathbf{g}^i \tag{23}$$

where $\widetilde{\mathbf{x}}_{,i}$ can be seen as an enhancement of $\mathbf{x}_{,i}$. We choose an $\widetilde{\mathbf{F}}$ which provides refined through-the-thickness kinematics, i.e.

$$\widetilde{\mathbf{x}}_{,i}\left(\alpha_i\left(\xi^1, \xi^2\right), \xi\right) = \begin{cases} \xi\,\alpha_3\left(\xi^1, \xi^2\right)\mathbf{d}\left(\xi^1, \xi^2\right) & \text{if } i = 3 \\ \mathbf{0} & \text{otherwise} \end{cases} \tag{24}$$

where α_i are enhancing parameters. We collect non-zero parameters in $\boldsymbol{\alpha}$, i.e. $\boldsymbol{\alpha} = \{\alpha_3\}$. The Green-Lagrange strains with respect to the basis $\mathbf{g}^i$ follow from $\mathbf{E} = \frac{1}{2}\left(\mathbf{F}^T\mathbf{F} - \mathbf{I}\right)$ and $\mathbf{I} = (\mathbf{X}_{,i} \cdot \mathbf{X}_{,j})\mathbf{g}^i \otimes \mathbf{g}^j$ as

$$E_{ij}\left(\boldsymbol{\Phi}_{EAS}, \boldsymbol{\alpha}, \xi\right) = \frac{1}{2}\left((\mathbf{x}_{,i} + \widetilde{\mathbf{x}}_{,i}) \cdot (\mathbf{x}_{,j} + \widetilde{\mathbf{x}}_{,j}) - \mathbf{X}_{,i} \cdot \mathbf{X}_{,j}\right) \tag{25}$$

It can be shown that all components of E_{ij} are quadratic with respect to ξ coordinate. This is in contrast with geometrically linear version of EAS from previous section where all strains were linear with respect to ξ coordinate, see (15) and (16). The strains (25) can be transformed to the local Cartesian frame with the basis (5), see (6), to obtain $\widehat{E}_{ij}$.

Assumption (22) is introduced into Hu-Washizu functional $\Pi_{H-W}\left(\mathbf{\Phi}_{EAS}, \widetilde{\mathbf{F}}, \mathbf{P}\right)$, where $\mathbf{P} = \mathbf{FS}$ is the first Piola-Kirchhoff stress tensor. The following functional is obtained

$$\Pi_{EAS2}\left(\mathbf{\Phi}_{EAS}, \boldsymbol{\alpha}\right) = \int_V W\left(\widehat{E}_{ij}\left(\mathbf{\Phi}_{EAS}, \boldsymbol{\alpha}, \xi\right)\right) dV - \Pi_{ext}\left(\mathbf{\Phi}_{EAS}\right) \tag{26}$$

if the orthogonality between $\mathbf{P}$ and $\widetilde{\mathbf{F}}$ is assumed to be valid

$$\int_V \mathbf{P} : \widetilde{\mathbf{F}} dV = 0 \tag{27}$$

By noting that $\mathbf{g}^3 = \mathbf{g}_3 = \mathbf{g}$, and by using (23) and (24), it follows from (27)

$$\begin{aligned}
\int_V \mathbf{P} : \left(\widetilde{\mathbf{x}}_{,3} \otimes \mathbf{g}^3\right) dV &= \int_V \mathbf{P} : \left(\mathbf{d} \otimes \mathbf{g}\right) \xi \alpha_3 dV \\
&= \int_A \alpha_3 \int_{-h/2}^{h/2} \mathbf{d} \cdot \mathbf{Pg} \underbrace{\left(1 - 2\xi H + (\xi)^2 K\right)}_{\mu} \xi d\xi dA \\
&= 0
\end{aligned} \tag{28}$$

Equation (28) holds for shells with $\mu \approx 1$ for constant product $\mathbf{d} \cdot \mathbf{Pg}$ with respect to the through-the-thickness coordinate ξ. It also holds for shells with $H = const.$, $K = const.$ when product $\mathbf{d} \cdot \mathbf{Pg}$ is only function of ξ, if α_3 is chosen such that $\int_A \alpha_3 dA = 0$.

One can introduce variations of displacement $\mathbf{u} \to \mathbf{u} + \varepsilon \delta \mathbf{u}$, shell director rotation $\mathbf{a}(\boldsymbol{\vartheta}) \to \mathbf{a}(\boldsymbol{\vartheta} + \varepsilon \delta \boldsymbol{\vartheta})$, thickness stretching parameter $\widetilde{\lambda} \to \widetilde{\lambda} + \varepsilon \delta \widetilde{\lambda}$, and enhancing parameters $\boldsymbol{\alpha} \to \boldsymbol{\alpha} + \varepsilon \delta \boldsymbol{\alpha}$. Those variations are then introduced in Π_{EAS2} to obtain $G_{EAS2} = \frac{d\Pi_{EAS2}}{d\varepsilon}|_{\varepsilon=0}$. At the stationary point

$$G_{EAS2}\left(\delta\mathbf{\Phi}_{EAS}, \delta\boldsymbol{\alpha}; \mathbf{\Phi}_{EAS}, \boldsymbol{\alpha}\right) = 0 \tag{29}$$

the equilibrium and kinematic relations are fulfilled in a weak form. This functional is further solved by the finite element approximation. Since $\boldsymbol{\alpha}$ parameters need not to be continuos over the domain, they are condensed on the element level, and the method can fit nicely within the standard finite element assembly.

2.4   Linearized formulations

To get consistently linearized forms of the above described versions of 3-d shell formulation, we linearize functionals (12), (21) and (29) about the initial configuration.

The initial configuration of version 1 is defined by $\boldsymbol{\Phi} = \left\{ \mathbf{u}, \boldsymbol{\vartheta}, \widetilde{\lambda}, q \right\} = \mathbf{0}$. The perturbation of initial configuration can be defined with displacement $\mathbf{u} \to \varepsilon \Delta \mathbf{u}$, shell director rotation $\mathbf{a}(\boldsymbol{\vartheta}) \to \mathbf{a}(\varepsilon \Delta \boldsymbol{\vartheta})$, and thickness stretching parameters $\widetilde{\lambda} \to \varepsilon \Delta \widetilde{\lambda}$, $q \to \varepsilon \Delta q$. When introducing those expressions into the weak form of equilibrium equations (12), one can get its consistently linearized form around the initial configuration as

$$G_{Lin}\left(\delta\boldsymbol{\Phi}; \Delta\boldsymbol{\Phi} \right) = \frac{dG\left(\delta\boldsymbol{\Phi}; \boldsymbol{\Phi} \right)}{d\varepsilon} \big|_{\varepsilon=0} = 0 \tag{30}$$

The initial configuration of versions 2 and 3 is defined by $\boldsymbol{\Phi}_{EAS} = \left\{ \mathbf{u}, \boldsymbol{\vartheta}, \widetilde{\lambda}, q \right\} = \mathbf{0}$ and $\boldsymbol{\alpha} = \mathbf{0}$. The perturbation of initial configuration can be defined with displacement $\mathbf{u} \to \varepsilon \Delta \mathbf{u}$, shell director rotation $\mathbf{a}(\boldsymbol{\vartheta}) \to \mathbf{a}(\varepsilon \Delta \boldsymbol{\vartheta})$, thickness stretching parameter $\widetilde{\lambda} \to \varepsilon \Delta \widetilde{\lambda}$, and enhancing parameters $\boldsymbol{\alpha} \to \varepsilon \Delta \boldsymbol{\alpha}$. When those expressions are introduced into the functionals $G_{EAS1}\left(\delta\boldsymbol{\Phi}_{EAS}, \delta\boldsymbol{\alpha}; \boldsymbol{\Phi}_{EAS}, \boldsymbol{\alpha} \right) = 0$ and $G_{EAS2}\left(\delta\boldsymbol{\Phi}_{EAS}, \delta\boldsymbol{\alpha}; \boldsymbol{\Phi}_{EAS}, \boldsymbol{\alpha} \right) = 0$, one gets their consistently linearized forms as

$$G_{EAS1,Lin}\left(\delta\boldsymbol{\Phi}_{EAS}, \delta\boldsymbol{\alpha}; \Delta\boldsymbol{\Phi}_{EAS}, \Delta\boldsymbol{\alpha} \right) = \frac{dG_{EAS1}\left(\delta\boldsymbol{\Phi}_{EAS}, \delta\boldsymbol{\alpha}; \boldsymbol{\Phi}_{EAS}, \boldsymbol{\alpha} \right)}{d\varepsilon} \big|_{\varepsilon=0} = 0 \tag{31}$$

$$G_{EAS2,Lin}\left(\delta\boldsymbol{\Phi}_{EAS}, \delta\boldsymbol{\alpha}; \Delta\boldsymbol{\Phi}_{EAS}, \Delta\boldsymbol{\alpha} \right) = \frac{dG_{EAS2}\left(\delta\boldsymbol{\Phi}_{EAS}, \delta\boldsymbol{\alpha}; \boldsymbol{\Phi}_{EAS}, \boldsymbol{\alpha} \right)}{d\varepsilon} \big|_{\varepsilon=0} = 0 \tag{32}$$

In practice, one needs to consistently linearize the strains $\widehat{E}_{ij} = \widehat{E}_{ij}(\boldsymbol{\Phi})$ (for version 1) and the strains $\widehat{E}_{ij} = \widehat{E}_{ij}(\boldsymbol{\Phi}_{EAS}, \boldsymbol{\alpha})$ (for versions 2 and 3) as well as the corresponding functional related to the external loading, i.e. $\delta\Pi_{ext}(\delta\boldsymbol{\Phi}, \boldsymbol{\Phi})$ or $\delta\Pi_{ext}(\delta\boldsymbol{\Phi}_{EAS}, \boldsymbol{\Phi}_{EAS})$.

3   Numerical examples

For the finite element approximation of the above presented 3d-shell formulations we used 4-node isoparametric elements with assumed natural strain (ANS) interpolation [Bathe and Dvorkin (1985)] for the transverse shear strains. Details on numerical implementation of geometrically nonlinear versions are presented in Brank, Korelc and Ibrahimbegovic (2002) and Brank (2005); see also Brank (2008) for the assessment of EAS-ANS 4-node elements based on classical shell kinematics.
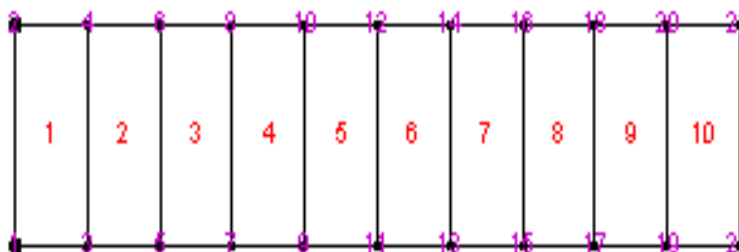
Figure 1: Mesh of 10×1 elements.

In this section we present results of several numerical simulations, which can illustrate the ability of the derived 3d-shell formulations to accurately predict 3d stress state in elastic plates and shells. The stresses for versions 2 and 3 have been computed by using constitutive equations.

All the finite element codes have been produced by using symbolic program Ace-Gen [Korelc (2008)], which has been developed for automatic generation of finite element codes [Korelc (1997)]. The computations have been carried out by the accompanying computer code AceFem [Korelc (2008)].

3.1 Cantilever plate

With this example we illustrate the ability of the above presented linearized formulations to (A) produce zero transverse normal stresses in the case of pure bending, and (B) to present more general stress state in the case of general bending problem.

We consider a cantilever plate with the following geometric and material data: length $L = 1$, width $W = L/4$, thickness $h = L/10$, $E = 2 \times 10^8$, $v = 0.3$. The chosen mesh contains 10×1 elements, see Figure 1. The axis 1 is parallel to the longitudinal axis of the cantilever, the axis 2 is perpendicular to 1 and parallel to the cantilever mid-plane, and axis 3 is perpendicular to the cantilever mid-plane. The number of mid-surface Gauss integration points is 4. The number of through-the-thickness Gauss integration points, located at different ξ positions at ξ^1 and ξ^2 locations of the mid-surface Gauss points, is 10. This is an overkill for accuracy, but employed nonetheless in order to get clear presentation of through-the-thickness variation of stresses. The supported edge is soft clamped with free higher-order degrees of freedom. The loading cases are two: (A) moment $M = 100$ at the free end of the cantilever, and (B) uniform pressure $p = 1000$ at the plate top surface (at $\xi = h/2$).

Load case A. For the pure bending load case A the only non-zero computed stress
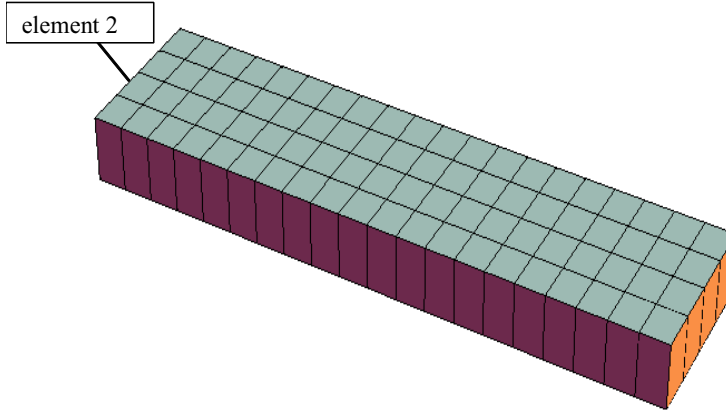
Figure 2: Mesh of 20×4 elements presented with plate thickness.

for all three versions of 3d-shell formulation is S^{11}. All other computed stresses, including S^{33}, are indeed equal to zero. The corresponding solutions for strain field components are in complete accordance with the linear elasticity and they suggest that the considered formulations are not affected by the so called Poisson's ratio locking effect that occurs without through-the-thickness enhancement [Büchter, Ramm and Roehl (1994); Bischoff and Ramm (1997)].

We note that in case of mid-surface application of loading on plate (as in the load case A) the higher-order kinematic parameter $\widetilde{\lambda}$ is not activated and it remains equal to zero.

Load case B; mesh is 10×1 elements. For the load case B we get richer stress state. In Figures 3 to 7 we show the distribution of stresses through the thickness. The stresses S^{11}, S^{12}, S^{13} and S^{33} are presented either (a) for the mid-surface Gauss-point closest to the supported edge or (b) as averaged values at each "through-the-thickness Gauss point layer" of the element closest to the supported edge. It can be seen from Figures 3 to 7 that the solutions of different formulations differ from one another. For example, S^{13} and S^{33} are constant for versions 2 and 3; S^{33} equals to $-p/2$. On the other hand, S^{33} of version 1 shows clear tendency of going towards $-p$ at the top surface and towards 0 at the bottom surface, with its average through-the-thickness value of $-p/2$. The stress S^{13} of version 1 varies quadratically through the thickness, but it is not equal to zero at top and bottom surfaces. This suggests that shear correction factors should be used for all formulations.

The stresses S^{22} (for all three versions) and S^{33} (for version 1) are presented as averaged values at each "layer" at a particular value of through-the-thickness coor-

dinate ξ. The reason for element-wise averaging of S^{22} and S^{33} stresses in Figures 6 to 7 are their oscillations throughout an element at each "layer". Those oscillations include the sign change as shown in Figures 8 and 9. It is thus reasonable to interpret those stresses throughout an element with their averaged values.

We note that the tip displacement/rotation is practically identical for all the versions; the computed values are 0.00757/0.01007 for version 1 and 0.00756/0.01005 for versions 2 and 3. Hence, just reporting on the displacement values does not reveal much on the predictive capabilities of these shell formulations.

Load case B; mesh is 20×4 **elements.** In order to check the influence of the mesh on the results, we refine the mesh to 20×4 elements. This refinement does not change the displacements; compare the results in Figures 10 and 11. The dispersion of values at different Gauss points of the same element did not improve. On the contrary, the dispersion gets even worse; see Figure 12 for the results obtained for S^{33} for the element 2 (Fig. 2). It can be clearly seen that even "layer-wise" element averaging does not lead to reasonable results. The only reasonable averaging in this case is through-the-thickness averaging of S^{33} at each mid-surface integration point, which leads to $S^{33} \approx -p/2$.

3.2 Thick cylinder

With this example we test ability of the above presented linearized 3d-shell formulations to predict through-the-thickness distribution of radial and circumferential stresses in a thick cylindrical shell. We consider thick cylinder in the plain strain state with the following geometrical and material data: radius of middle surface $R = 1$, width $L = 2R\pi/4$, thickness values $h = 0.1$ (cylinder 1; $R/h = 10$) and $h = 0.2$ (cylinder 2; $R/h = 5$), $E = 3 \times 10^7$, $\nu = 0.2$. The applied load is internal pressure $p = 1000$. The finite element mesh consists of 32×1 elements for discretization of the whole cylinder, see Figure 13. To simulate the plain strain state we set axial displacement of all nodes of the mesh to zero.

Radial displacements of points at R are presented in Table 1 for cylinder 1 with $R/h = 10$ and cylinder 2 with $R/h = 5$. The computed results match very well. We can see that the formulation 1 (with 7 displacement-like kinematic parameters) and formulation 3 (with the corresponding additive split of displacement gradient) are able to match analytic solution somewhat better than formulation 2 (additive split of strains).

We then turn to the accuracy of stress computation. We first consider results for cylinder 1. Through-the-thickness distribution of radial and circumferential stresses are compared with analytical solutions as shown in Figures 14 and 15. It can be seen from Figures 14 and 15 that circumferential stresses of all formulations match
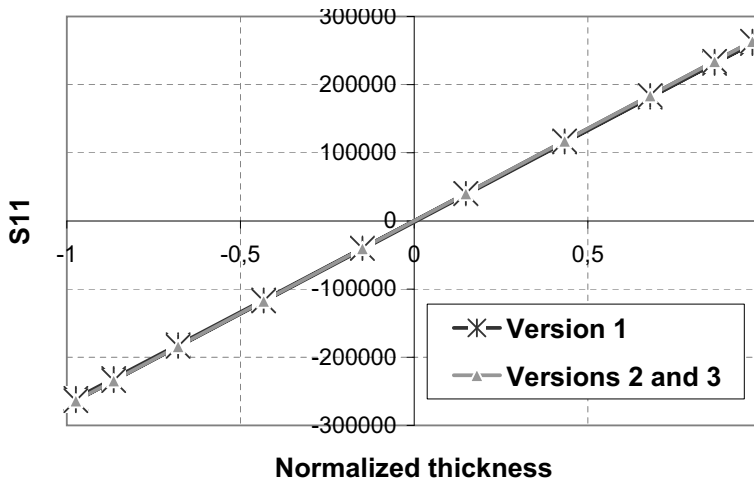
Figure 3: Through-the-thickness variation of S^{11} at the mid-surface Gauss-point closest to the supported edge.
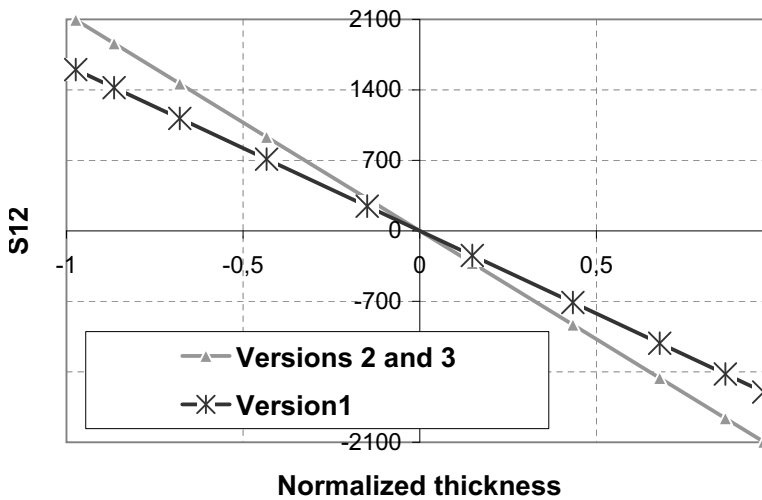

Figure 4: Through-the-thickness variation of S^{12} at the mid-surface Gauss-point closest to the supported edge.
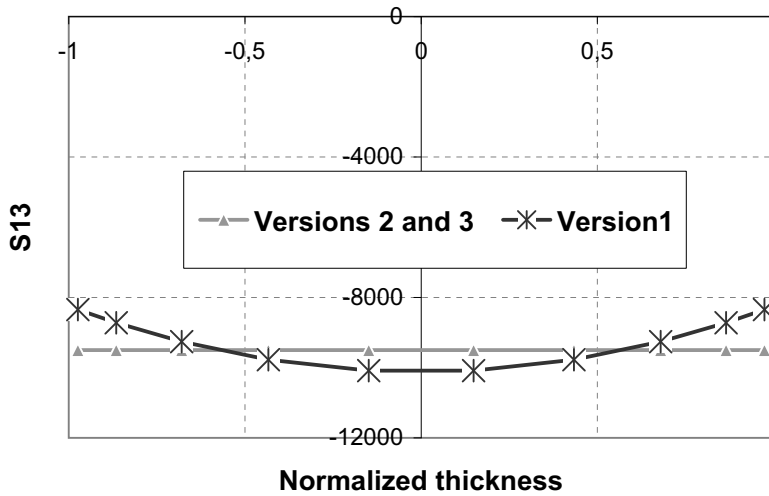
Figure 5: Through-the-thickness variation of S^{13} at the mid-surface Gauss-point closest to the supported edge.
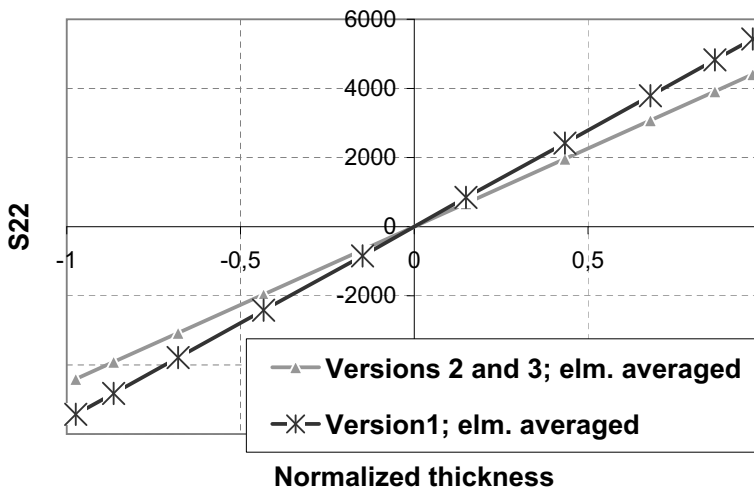

Figure 6: Through-the-thickness variation of S^{22}. "Layer-wise" averaged for the element closest to the supported edge.
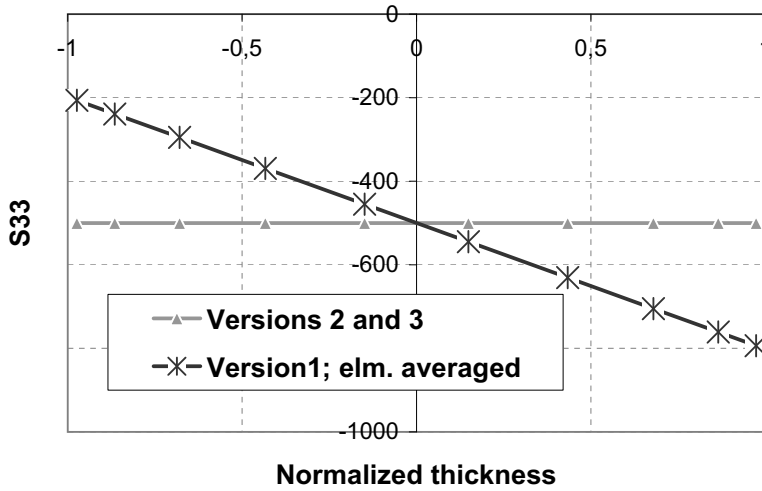
Figure 7: Through-the-thickness variation of S^{33}. "Layer-wise" averaged for the element closest to the supported edge (version 1). Values at the mid-surface Gauss-point closest to the supported edge (versions 2 and 3).
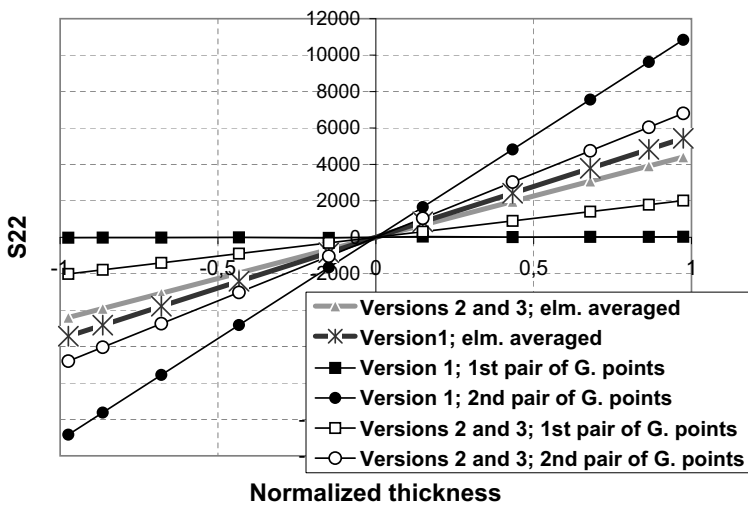
Figure 8: Through-the-thickness variation of S^{22} at the element closest to the supported edge.
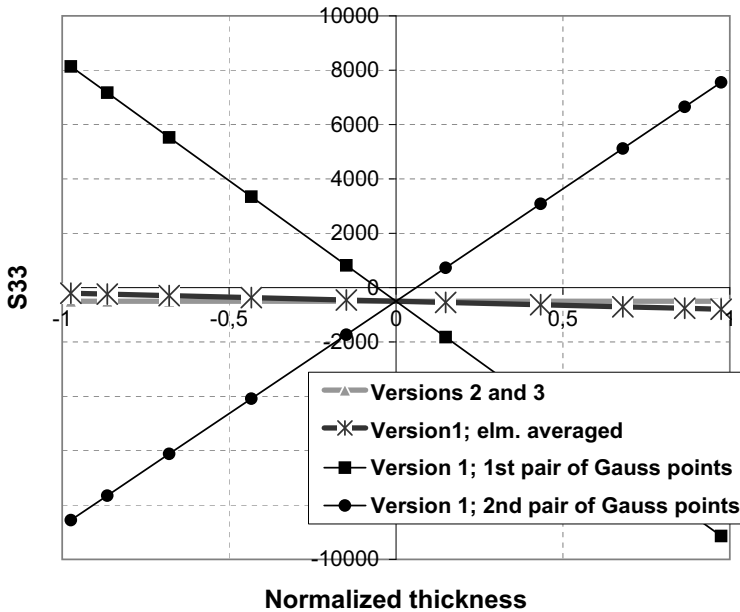
Figure 9: Through-the-thickness variation of S^{33} at the element closest to the supported edge.

analytical solution very well (maximum difference is only 1.5%). On the other hand, the through-the-thickness nonlinearity of radial stresses is well represented only by version 1, which has the ability of global representation of the through-the-thickness strain field. The computed results for version 2 and version 3 predict the radial stress, which is almost constant through the thickness with a value roughly equal to the average. Hence we can not have true stress distribution with enhanced strain (or incompatible modes) based 3-d shell elements everywhere, but we can have the (average) values which match the true distribution at the point with optimal accuracy.

The results for cylinder 2 are presented in Figures 16 and 17. It can be seen that for increased thickness the trend of the solution is similar as before, however, the difference between analytical and computed solutions will increase even further.

4   Conclusions

The modern developments on higher-order shell formulations, which employ extra parameters in order to properly account for the linear variation of through-the-
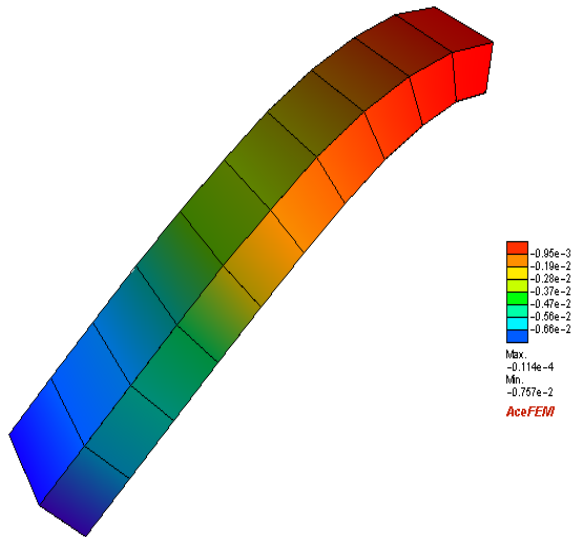
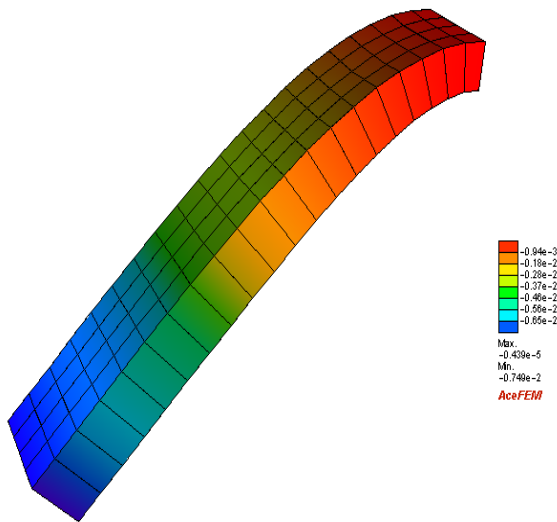Figure 10: 3d representation of plate displacements for version 1 (magnified 120 times) for mesh of 10×1 elements.

Figure 11: 3d representation of plate displacements for version 1 (magnified 120 times) for mesh of 20×4 elements.
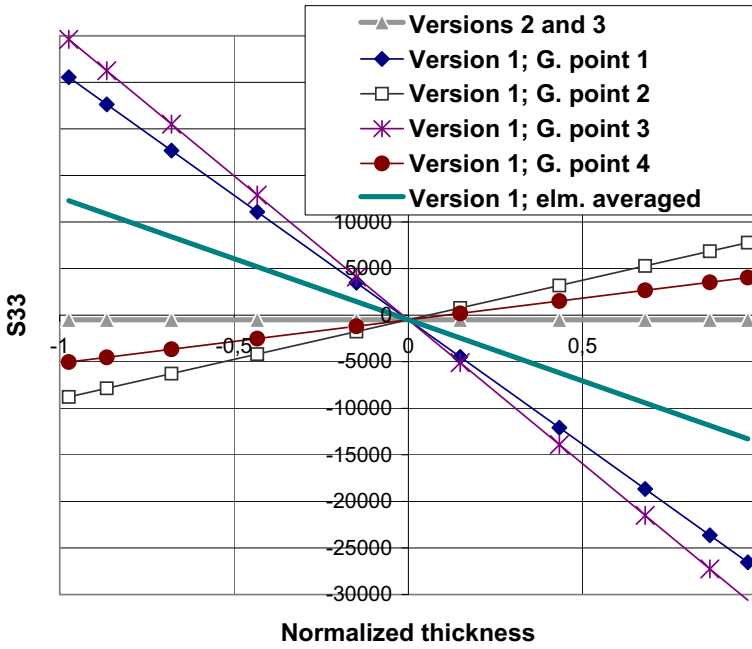
Figure 12: Through-the-thickness variation of S^{33} at the element 2 (see Fig. 2). Mesh is of 20×4 elements.
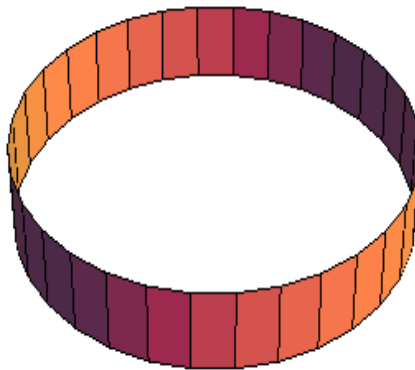

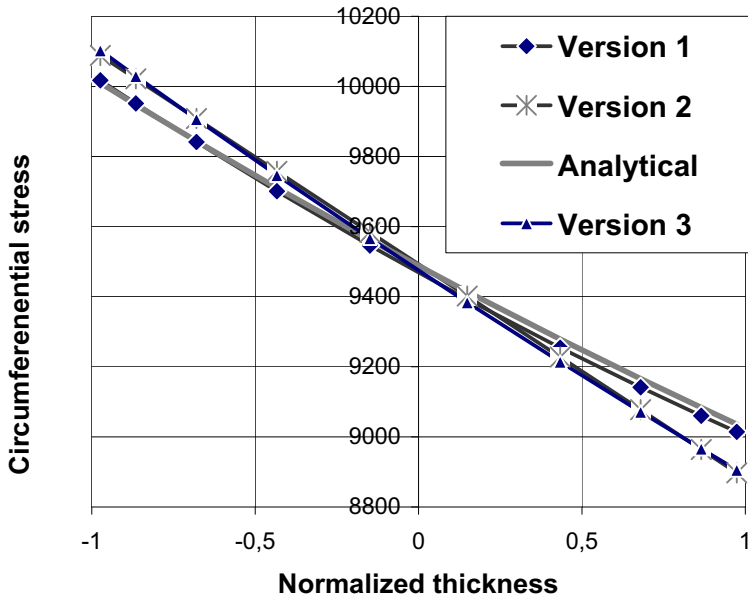Figure 13: FE mesh for analysis of thick cylinder.

Figure 14: Thick cylinder 1: Variation of circumferential stress in the thickness direction.
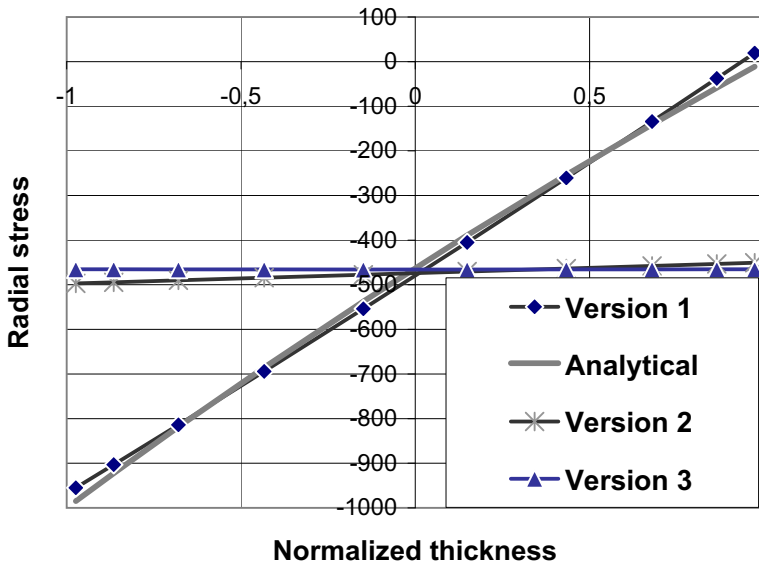

Figure 15: Thick cylinder 1: Variation of radial stress in the thickness direction.
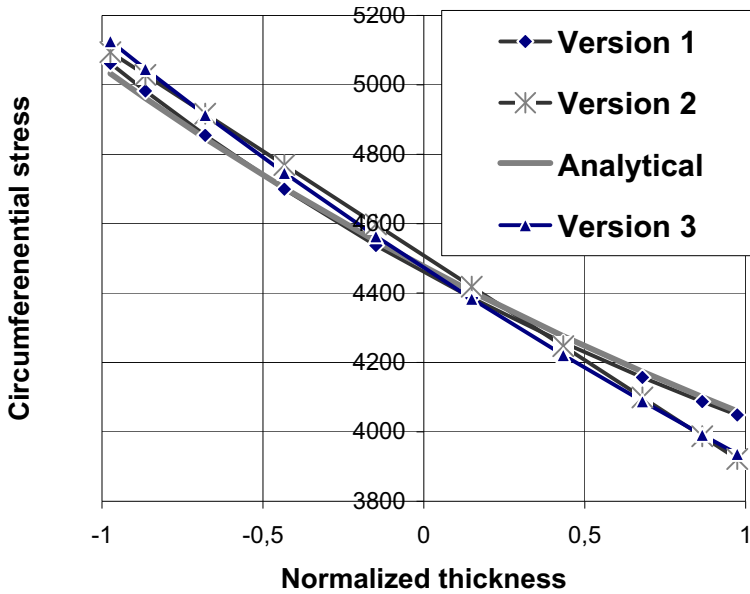
Figure 16: Thick cylinder 2: Variation of circumferential stress in the thickness direction.
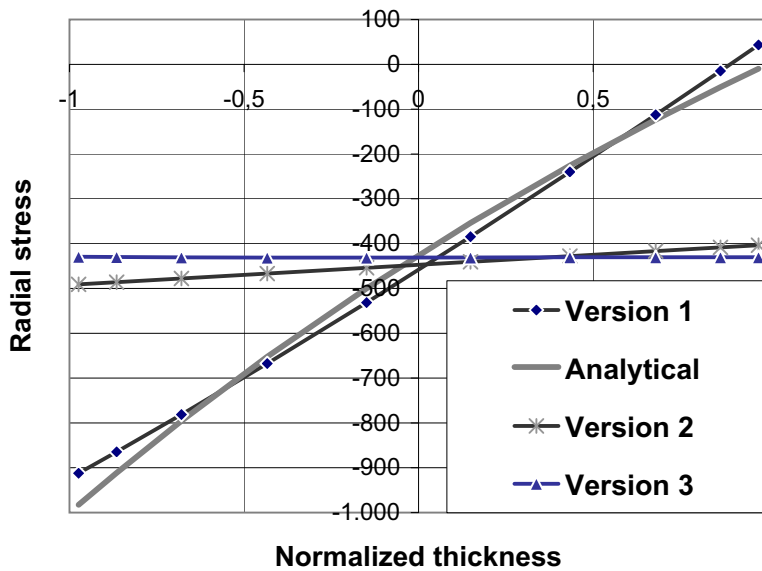

Figure 17: Thick cylinder 2: Variation of radial stress in the thickness direction.

Table 1: Radial displacement of the middle surface $\times 10^4$

	Version 1	Version 2	Version 3	Analytical
Cylinder 1	3.0682	3.0376	3.0691	3.0730
Cylinder 2	1.4637	1.4784	1.4656	1.4661

thickness stretch, indeed provide the benefit of being able to use fully 3d constitutive equations, the same as those for 3d continuum mechanics solid model. However, as shown in this work, this does not imply the same accuracy for the computed stress components as for the 3d continuum case, even though in both cases the stress tensor would have all the stress components defined.

We have shown by computed results that the dominant stress tensor components are predicted with high accuracy, especially those that are predicted by typical shell-like behavior (e.g. bending modes). The remaining stress components does not follow the same trend of high accuracy computations. For example the stress component in the transverse direction to bending axis, or yet the through-the-thickness stress (the main "acquisition" of this kind of higher-order shells), will both have somewhat erratic dispersion of results within a single element, which might be the consequence of the directional character of the shell element interpolations (in sharp difference with "isotropic" character of the standard isoparametric interpolations for 3d solids).

In this work, we have shown that the simple averaging procedure of the non-dominant stress components for all the Gauss points within the corresponding "layer" produces much improved results. It is important to note that this cure is more efficient than the mesh refinement. We have also shown that it might happen that the "layer-wise" averaging of S^{33} over an element is not effective. In that case S^{33} should be averaged through the shell thickness.

Among three different shell models we discussed, the best results are always obtained by the model with seven displacement-like kinematic parameters (version 1), which, on the other hand, has a serious disadvantage of having two additional global degrees of freedom with respect to standard shell formulation with Reissner-Mindlin kinematics. Also, through-the-thickness variation of some non-dominant stresses may be computed very inaccurately, so that they can be correctly interpreted either by "layer-wise" element averaging or by through-the-thickness averaging.

Two EAS versions of the higher-order shell formulation (version 2 and version 3) have only one additional global degree of freedom with respect to standard shell formulation, and can easily fit within the standard finite element computer program

structure, but reduce further the stress results accuracy. Namely, although version 3 is systematically better than version 2, neither can provide the exact distribution of through-the-thickness stress. However, we can obtain the good prediction for the average value at the point of optimal accuracy at shell mid-surface. This indicates a potential benefits we could have for assumed stress interpolation which can be proposed with desired stress variation and enforced to match the computed average values.

Reference

Atluri, S. N.; Cazzani, A. (1995): Rotation in computation solid mechanics, *Archives of Computational Methods in Engineering*, vol. 2, pp. 49-138.

Bathe, K. J.; Dvorkin, E. (1985): A four-node plate bending element based on Mindlin-Reissner plate theory and a mixed interpolation, *Int J Numer Meth Engng*, vol. 21, pp. 367-383.

Başar, Y.; Itskov, M.; Eckstein, A. (2000): Composite laminates: Nonlinear inter-laminar stress analysis by multi-layer shell elements, *Comput Methods Appl Mech Engrg*, vol. 185, pp. 367-397.

Betsch, P.; Gruttmann, F.; Stein, E. (1996): A 4-node finite shell element for the implementation of general hyperelastic 3d-elasticity at finite strain, *Comput Methods Appl Mech Engrg*, vol. 130, pp. 57-79.

Bischoff, M; Ramm, E. (1997): Shear deformable shell elements for large strains and rotations, *Comput Methods Appl Mech Engrg*, vol. 40, pp. 4427-4449.

Brank, B (2005): Nonlinear shell models with seven kinematic parameters, *Comput Methods Appl Mech Engrg*, vol. 194, pp. 2336-2362.

Brank, B.; Ibrahimbegovic, A. (2001): On the relation between different parametrizations of finite rotations for shells, *Engineering Computations,* vol. 18, pp. 950-973.

Brank, B.; Korelc, J.; Ibrahimbegovic, A. (2002): Nonlinear shell problem formulation accounting for through-the-thickness stretching and its finite element implementation, *Computers and Structures*, vol. 80, 699-717.

Brank, B. (2008): Assessment of 4-node EAS-ANS shell elements for large deformation analysis, *Comput Mech*, vol. 42, pp. 39-51.

Büchter, N.; Ramm, E.; Roehl, D. (1994): Three-dimensional extension of non-linear shell formulation based on the enhanced assumed strain concept, *Int J Numer*

Meth Engng, vol. 37, pp. 2551–2568.

Eberlein, R.; Wriggers, P. (1999): Finite element concepts for finite elastoplastic strains and isotropic stress response in shells: theoretical and computational analysis, *Comput Methods Appl Mech Engrg*, vol. 171, pp. 243-279.

Ibrahimbegovic, A.; Wilson, E. I. (1991): A modified method of incompatible modes, *Commun Numer Methods Engng*, vol. 8, pp. 23-32.

Ibrahimbegovic, A.; Frey, F. (1993): Geometrically non-linear method of incompatible modes in application to finite elasticity with independent rotations, *Int J Numer Methods Engng*, vol. 36, pp. 4185-4200.

Korelc, J. (1997): Automatic generation of finite element code by simultaneous optimization of expressions, *Theor Comput Sci,* vol. 187, pp. 231-248.

Korelc, J. (2008): AceGen, AceFem, available at http://www.fgg.uni-lj.si/Symech.

Kulikov, G. M.; Plotnikova, S. V. (2008): Finite rotation geometrically exact four-node solid-shell element with seven displacement degrees of freedom, *CMES: Computer Modeling in Engineering & Sciences*, vol. 28, pp. 15-38.

Krätzig, W. B.; Jun, D. (2003): On 'best' shell models - from classical shells, degenerated and multilayered concepts to 3D, *Archive of Applied Mechanics*, vol. 73, pp. 1-25.

Lin, C. S. (2006): The computations of large rotation through an index two nilpoint equation, *CMES: Computer Modeling in Engineering & Sciences*, vol. 16, pp. 157-175.

Rössle, A.; Bischoff, M.; Wendland, W.; Ramm, E. (1999): On the mathematical foundation of the (1,1,2)-plate model, *Int J Solids and Struct,* vol. 36, pp. 2143-2168.

Sansour, C. (1995): A theory and finite element formulations of shells at finite deformations involving thickness change: circumventing the use of the rotation tensor, *Arch Appl Mech*, vol. 65, pp. 194-216.

Simo, J. C.; Rifai, S. (1990): A class of mixed assumed strain methods and the method of incompatible modes, *Int J Numer Meth Engng,* vol. 29, pp. 1595-1638.

Simo, J. C., Armero, F. (1992): Geometrically non-linear enhanced strain mixed methods and the method of incompatible modes, *Int J Numer Meth Engng*, vol. 33, pp. 1413-1449.

Tonković, Z.; Sorić, J.; Skozrit, I. (2008): On numerical modeling of cyclic elastoplastic response of shell structures, *CMES: Computer Modeling in Engineering & Sciences*, vol. 26, pp. 75-90.

Wen, P. H., Hon; Y. C. (2007): Geometrically nonlinear analysis of Reissner-

Mindlin plate by meshless computation, *CMES: Computer Modeling in Engineering & Sciences*, vol. 21, pp. 177-191.